A new route of magnetic biochar based polyaniline composites for supercapacitor electrode materials

Article *in* Journal of Analytical and Applied Pyrolysis · August 2016

DOI: 10.1016/j.jaap.2016.08.004

5 authors, including:

Thines Raj Kogiladas
Universiti Teknologi Malaysia
12 PUBLICATIONS **46** CITATIONS
SEE PROFILE

Ezzat Chan Abdullah
UNIVERSITI TEKNOLOGI MALAYSIA
87 PUBLICATIONS **684** CITATIONS
SEE PROFILE

Mubarak N Mujawar
Curtin University Sarawak
66 PUBLICATIONS **405** CITATIONS
SEE PROFILE

Manoj Tripathi
University of Malaya
11 PUBLICATIONS **87** CITATIONS
SEE PROFILE

Journal of Analytical and Applied Pyrolysis xxx (2016) xxx–xxx

Contents lists available at ScienceDirect

Journal of Analytical and Applied Pyrolysis

journal homepage: www.elsevier.com/locate/jaap

A new route of magnetic biochar based polyaniline composites for supercapacitor electrode materials

K.R. Thines [a], E.C. Abdullah [a,*], M. Ruthiraan [a], N.M. Mubarak [b,*], Manoj Tripathi [c]

[a] Malaysia-Japan International Institute of Technology (MJIIT), Universiti Teknologi Malaysia, Jalan Semarak, 54100 Kuala Lumpur, Malaysia
[b] Department of Chemical Engineering, Faculty of Engineering and Science, Curtin University, 98009 Sarawak, Malaysia
[c] Department of Mechanical Engineering, Faculty of Engineering, University of Malaya, 50603 Kuala Lumpur, Malaysia

ARTICLE INFO

Article history:
Received 12 May 2016
Received in revised form 18 July 2016
Accepted 5 August 2016
Available online xxx

Keywords:
Magnetic biochar
Polyaniline
Durian's rind
Vacuum pyrolysis
In-situ polymerization
Specific capacitance

ABSTRACT

In this paper, abundantly available durian's rind was opted as raw material to synthesize magnetic biochar in the presence of three different metallic salts by employing a novel vacuum condition in an electrical muffle furnace. Magnetic biochar was successfully produced with a maximum BET surface area value of 835 m^2/g at the pyrolysis temperature and time of 800 °C and 25 min. This magnetic biochar was successfully employed to support and disperse polyaniline (PANI) particles for the application as supercapacitor electrode materials. The produced magnetic biochar – PANI composite exhibited an enhanced specific capacitance compared to the pure PANI and magnetic biochar. The highest specific capacitance of 615 F/g at 10 mV/s and energy density of 76.88 Wh/kg were demonstrated by the MBCA composite, which is considered favorably high compared to the existing PANI coated carbon composites. This magnetic biochar – PANI composites exhibits a good potential for future supercapacitor applications.

1. Introduction

A well-known futurist, Ray Kurzweil stated that "We won't experience 100 years of progress in the 21st century, it will be more like 20,000 years of progress at today's rate", back in the year 2001 [1]. This statement acknowledges the growth of technology we are going through in this modernization era. The introduction of the wireless internet, smartphones, Facebook, and Twitter proves how much things have changed in the past 10 years. Hence, these examples can predict on how vastly different things will be in the upcoming 10 or 100 years. The development of a smartphone from a telephone booth shows that the idea of technology is getting bigger while the silicon transistors being used in the gadgets are getting smaller. This transformation shows that innovative ideas can be generated and achieved for the development of the nation. As for the nanotechnology sectors, robots can get smaller and smaller till they will be able to insert it into bodies to repair damaged tissues. On the other hand, energy generation issue can be solved by increasing the generation of solar power due to the growth in the nanotechnology sector. The famous quote by Neil Armstrong, "That's one small step for man, one giant leap for mankind" is proven day by day through new discovery throughout the world.

One of the important elements in the electronic industry would be the microelectronics field in which it utilizes tiny or micro components to manufacture electronics. The first integrated circuit was fabricated back in the year 1960s during the electronics revolution [2] and the industry has grown intensely, resulting in a faster, smaller and cheaper integrated circuit [3–5]. The integrated circuit is generally comprised of conductors, semiconductors, capacitors, supercapacitors, and insulators attached to it in which the semiconductors act as the active device component [6–8]. On the other hand, conductors are commonly used on the integrated circuit to provide interconnection applications, for electrostatic discharge and for the electromagnetic interference of the electronic equipment. Insulators, on the other hand, are common polymers which are extensively used as encapsulants, materials for the packaging and housing of electronic equipment [7,8]. On the contrary, supercapacitors are generally used as an energy storage device which is receiving much attention due to its wide application in portable electronics, telecommunications, and intermittent electrical energy [9–11]. Thus, the material which being used in the electrode which enhances the energy storage capability is gaining much attention and research interest from energy storage and

* Corresponding authors.
E-mail addresses: thinesraj27@gmail.com (K.R. Thines), ezzatc@utm.my, ezzatchan@gmail.com (E.C. Abdullah), mubarak.mujawar@curtin.edu.my, mubarak.yaseen@gmail.com (N.M. Mubarak).

http://dx.doi.org/10.1016/j.jaap.2016.08.004
0165-2370/

materials science fields [12–15]. On par with this application of these devices, conducting polymers provides a unique combination of properties that can be used as a replacement in microelectronics.

Among various conductive polymer, polyaniline (PANI) exhibited a good performance as the supercapacitor electrode material due its influential properties such as high charge density, good electrical conductivity in various doped states, ease of fabrication for large-scale devices and low cost [16,17]. Generally, PANI exists in a form of green protonated emeraldine which is produced by the oxidative polymerization of aniline process in aqueous acids such hydrochloric acid, HCl, and this form was able to provide an electrical conductivity ranging from 10^{-2} to 10^{0} S/cm [18]. However, the application of PANI as the electrode in supercapacitor faced a downfall due to its large volumetric swelling and shrinking during the charge – discharge process due to ion doping and de – doping process. This downfall led to a structural breakdown and flaking off PANI [19,20]. One of the efficient ways to improve the electrochemical stability of PANI was by incorporating earth-abundant capacitive carbon materials such as graphene [21], ordered mesoporous carbon [22] and carbon nanotubes (CNT) [23]. The significant combination of essential mechanical strength of carbon material and high pseudocapacitance of the PANI stands out to be the contributing factor towards the high output energy of the produced electrode composite [16,20]. This effective combination of carbon material with PANI faced difficulty in terms of high cost, limited resource of raw material, and complicated preparation process [24–26]. Hence, low-cost carbon materials which were prepared from the abundantly available biomass resources were employed to produce carbon-PANI composites with significant capacitive performance as an electrode for supercapacitor materials.

In conjugation to that, durian's rind is found to be abundantly available in Malaysia with a significant advantage of environmentally friendly and low-cost. Although durian is largely consumed by Malaysians due to its prolific implementations, its demand hindered by the generation of huge amount of durian residues consisting of its shell, seeds, peels and rinds [27]. In order to avoid any environmental related issues due to the poor management of durian's rind, these rind were converted into biochar by heating at high temperatures under an inert or zero oxygen atmospheres to synthesize a low-cost biochar consisting of an impressive porous structure which favors better ion diffusion and electrolyte access, leading to a good electrochemical activity [28]. In recent years, durian's rind have been employed as an electrode's material for supercapacitors application which exhibited a good electrochemical performance [29]. However, there is only a few number of studies which focuses the application of metal derived biochar, or also known as magnetic biochar along with PANI as the electrode material for supercapacitors [30]. The magnetic biochar's properties such as high surface area and its ability of conducting electricity were found to enhance the capacitance value of the composite produced and ease the abundant loading of pseudocapacitive materials via serving as nucleation and anchoring sites [31].

Hence, motivated by these numerous interesting work, we successfully converted durian's rind into hematite and magnetite-loaded magnetic biochar by employing a novel vacuum condition in an electrical muffle furnace. This magnetic biochar was characterized to study its morphology and to detect the presence of hematite and magnetite. It was then used to synthesize the novel PANI coated hematite and magnetite doped biochar composite through an in-situ polymerization process in the presence of aniline monomer, magnetic biochar, and oxidant. These composites were fabricated as an electrode for supercapacitor and its electrical conductivity, capacitance and morphology were studied as well.

2. Materials and methods

2.1. Collection and grinding of raw material

Durian's rind was collected from a durian stall located in Kuala Lumpur. These durian's rinds were made sure not to be contaminated with fungus and in a dry condition when it was collected. The collected durian's rind was then were chopped into a smaller piece to ease the cleaning process. These durian's rind were then washed thoroughly to remove all the dirt from the rind and leftover durian on the inner part of rind while any durian's rind spotted with fungus were discarded. The washed durian rind was then dried in vacuum oven for 5 days continuously at 105 °C.

The grinding process was carried out at Forest Research Institute of Malaysia (FRIM) by employing a two-stage grinding process. The initial grinding process was done to obtain a particle with a size of less than 1 mm and the second grinding process was carried out to obtain particles with size less than 20 μm by employing the ball mill grinder through a continuous grinding and sieving process. The ground durian's rind particles were sieved to obtain a particle size of less than 20 μm and the grinding process is repeated until the required particle size is obtained. High yield of durian rind's particles was obtained by employing this two-stage grinding process due to the less lost in mass during the grinding. The ground durian's rind particles were then stored tightly in a sealed bag which was then placed in a desiccator.

2.2. Preparation of metal ion – durian's rind biomass

Analytical grade metal salt of iron (III) oxide, Fe_2O_3, iron (II) sulphate heptahydrate, $FeSO_4{\cdot}7H_2O$ and iron (III) chloride hexahydrate, $FeCl_3{\cdot}6H_2O$ along with ground durian's rind particles were used for the oxidization process to achieve a better porous structure at the surface of durian particles together with the attachment of carboxylic and carbonyl group on the surface of durian particles prior the pyrolysis process [32].

Initially, 200 mL of 1.0 M respective metal's ion salt solution were transferred into a 1L Pyrex laboratory bottle, followed by the addition of 150 mL of nitric acid, HNO_3 and 50 mL of potassium permanganate, $KMnO_4$ in the ratio of 3:1 as suggested by [33] for an optimum functionalization process. This solution was mixed uniformly prior the addition of 200 g of ground durian's rind particles into 400 mL mixture in 1 L Pyrex laboratory bottle. The mixture in the bottle was sonicated for 5 h at 40 °C with 50% vibration energy. The mixture was then dried in vacuum oven for 5 days continuously at a temperature of 70 °C to obtain the metal ion – durian rind biomass. The mixture was uniformly mixed every 6–10 h during the drying process to ensure a uniform drying throughout the particles. The dried biomass was then crushed using a mortar and pestle which were sieved later on to obtain particles with size less than 20 μm.

2.3. Synthesis of magnetic biochar

The prepared biomass was then used to produce magnetic biochar in a programmable muffle furnace model WiseTherm, FP-03, 1000 °C, 3 L with a vacuum condition. As can be seen from Fig. 1, a closed crucible containing the 50 g of dried biomass was kept in the middle of the furnace and the furnace door was closed tightly. The syngas effluent's tip at the top of the furnace was connected to a vacuum pump in which the air in the furnace will be sucked out to ensure a vacuum condition present in the furnace during the pyrolysis process. The control valve then will be closed tightly upon ensuring the pressure inside the muffle furnace reduces until a constant value in the pressure gauge is attained. The pyrolysis process was then carried out at 800 °C for 25 min. The muffle

Please cite this article in press as: K.R. Thines, et al., A new route of magnetic biochar based polyaniline composites for supercapacitor electrode materials, J. Anal. Appl. Pyrol. (2016), http://dx.doi.org/10.1016/j.jaap.2016.08.004

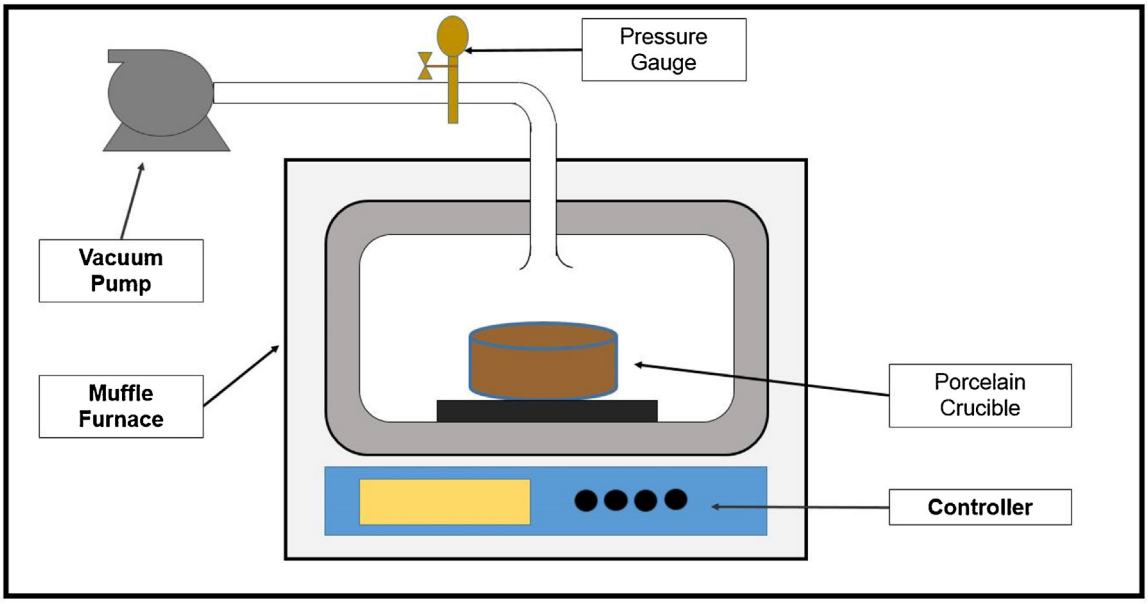

Fig. 1. Schematic of production of magnetic biochar by utilizing a muffle furnace.

furnace was allowed to cool down upon the pyrolysis process is complete until a room temperature condition is attained inside the furnace before the crucible was removed from the muffle furnace. The total amount of magnetic biochar produced was weighed. The magnetic biochar produced were rinsed with distilled water until a pH7 is obtained and then were dried in vacuum oven for 5 days at 70 °C. As for an easier discussion purpose, the magnetic biochar produced from iron (III) oxide, Fe_2O_3, iron (II) sulphate heptahydrate, $FeSO_4{\cdot}7H_2O$ and iron (III) chloride hexahydrate, $FeCl_3{\cdot}6H_2O$ metallic salt were denoted as MBO, MBS and MBC respectively.

2.4. Synthesis of magnetic biochar – PANI composite

Initially, MBO, MBS, and MBC was dissolved in 400 mL 1.0 M HCl solution and ultrasonicated over 3 h respectively to increase the solubility of magnetic biochar in HCl solution while aniline monomer was dissolved in 1.0 M HCl solution as well. Both mixtures were then transferred to a 1L beaker with an ice bath system which was placed on a magnetic stirrer. 200 mL of 1.0 M HCl solution containing 0.125 M ammonium persulfate (APS) was slowly added from burette to above suspension with constant mechanical stirring at 0–5 °C for 1 h. The reaction was further stirred for 2 h at 0–5 °C. The resulting suspension was filtered and rinsed several times with distilled water and methanol prior drying it at 60 °C for 24 h in a vacuum oven. As for easier discussion purpose, the aniline based magnetic biochar polymer composite were denoted as MBOA, MBSA, and MBCA.

2.5. Fabrication of supercapacitor electrodes

The magnetic biochar – polymer composite were fabricated into a bulk sample prior the electric conductivity measurement by employing the stainless steel mesh (400 pores per inch, 0.001 in. of wire and 38 μm of opening size). The surface contaminants of stainless steel mesh were cleaned prior by immersing it in acetone, 2 M HCl solution, ethanol solution and deionized water for 15 min. The MBOA, MBSA, and MBCA was created into a homogeneous paste by mixing it with acetylene black and polytetrafluoroethylene into the water in a mass ratio of 72:23:5 respectively [30]. These pastes were then pressed onto 1 cm^2 stainless steel current – collectors to produce various bulk samples.

2.6. Characterization of magnetic biochar and magnetic biochar – polymer composite

Field-emission scanning electron microscopy (FESEM) model Zeiss Auriga, Japan, was used to characterize the morphology of the magnetic biochar and its respective polymer composite. The surface area along with the pore size of magnetic biochar and its respective polymer composite was calculated using the Brunauer–Emmett–Teller (BET) equation through an Autosorb 1 surface area analyzer by nitrogen adsorption at 77 K (Brand: Quanta Chrome Model: Autosorb 6B). The attachment of the functional group and the presence of hematite and magnetite on the surface of magnetic biochar was determined by Fourier Transform Infrared (FTIR) spectroscopy (Brand: Bruker, Model: IFS66 v/S). Magnetic biochar – polymer composite also were examined by FTIR spectroscopy to determine the presence of PANI on the surface of magnetic biochar. The crystallinity structure and the presence of different type of elements in magnetic biochar and its respected polymer composite were determined by studying the XRD patterns (Model: Siemens D-500 X-ray, diffractometer, USA). The absorption peaks at a respective wavelength which can be used to determine the electron transition between the magnetic biochar and polymer chain were determined by UV–vis spectroscopy.

2.7. Electrical conductivity measurement

The electrical conductivity of MBOA, MBSA, and MBCA composite was determined by programmable DC voltage-current detector (Yokogawa, GS200). The conductivities of the polymer composite were measured according to equation 1 [34] as below in which V is the voltage difference, w is the width of the stainless steel mesh, t is the thickness of stainless steel mesh, I is the applied current and s is the electrode separation. The electrical conductivity of polymer composite was measured by varying the weight of magnetic biochar and aniline monomer. The sample with the highest electrical conductivity was then characterized by selected equipment and further analyzed through electrochemical measurement.

$$\sigma = (Vwt/Is) \quad (1)$$

Please cite this article in press as: K.R. Thines, et al., A new route of magnetic biochar based polyaniline composites for supercapacitor electrode materials, J. Anal. Appl. Pyrol. (2016), http://dx.doi.org/10.1016/j.jaap.2016.08.004

2.8. Electrochemical measurement

The CV curve of magnetic biochar and its respected polymer composite was determined and analyzed by using a three electrode electrochemical cell at room temperature consisting of silver–silver chloride (Ag/AgCl) as a reference electrode, platinum rod as the counter electrode while the magnetic biochar and its respected polymer composite's pellet as the working electrode dipped in 0.1 M potassium nitrate, KNO_3 solution. This electrochemical study was focused on the polymer composite which attained highest electrical conductivity value in the prior section in which the CV curve analysis and C_S value were determined by using Autolab Potentiostat PGSTAT302N. The voltage range for CV curve was set to −0.1 to 0.9 V at a scan rate of 10, 20, 30, 50 and 100 mV/s. The C_S (F/g) value of the polymer composite were determined from the CV curve by employing equation 2 [35] in which I (A) is the response current, V (V) is the applied potential, ΔV (V) is the potential window, v (mV/S) is the potential scan rate and m (g) is the mass of active material in the electrode. The determination of C_S value was followed by the calculation of energy density, E (Wh/kg) by utilizing Eq. (3).

$$C_S = \left(\int IdV\right)/vm\Delta V \quad (2)$$

$$E = 0.5 \times C_S \times V^2 \quad (3)$$

3. Results and discussion

3.1. Characterization of magnetic biochar and magnetic biochar – polymer composite

3.1.1. Field-emission scanning electron microscopy (FESEM)

The surface physical morphology of raw durian's rind, biochar, magnetic biochar, and its respected polymer composite was examined by FESEM. In accordance to that, Fig. 2 demonstrates the FESEM images of (a, b) raw durian's rind and (c, d) biochar at two different magnification scales of 50 and 1 μm. As can be seen from Fig. 2(a) and (b), it clearly indicates that raw durian's rind has an unsmooth surface with thin sheet consists of a structure of irregular shape throughout the ground sample. Besides that, there is no sign of pores formation on the surface of raw durian's rind [36]. Furthermore, Fig. 2(c) and (d) shows that a small number of macropores are found on the surface of biochar which was pyrolyzed at 800 °C for 25 min without the sonication process. The formation of micropores and macropores on the surface of biochar is attributed solely to the release of volatile matter during the pyrolysis process in the vacuum condition [36]. The biochar also found to exhibit a structure of highly conjugated aromatic sheets cross-linked in a random manner. Apart from that, the formation of tiny pores on the surface of biochar is related to the chemical decomposition of water and other organic substances which reduce the synthesis yield [37].

On the other hand, Fig. 3 exhibits the FESEM images of (a, b) MBO (c, d) MBS and (e, f) MBC at two different magnification scales of 50 and 1 μm. These images indicate that pyrolysis process in the muffle furnace with a vacuum condition initiated the formation of pores of different size and shapes on the surface, which leads to a formation of mesopores and micropores. The formation of series of rough cavities over the surface of durian's rind was more related to the breakdown of lignocellulosic material at high temperature, resulting in evaporation of volatile compounds away from the newly formed pores [38]. Furthermore, longer heating duration also cause some pores to become larger or eventually collapse which indirectly leads to a reduction in surface area [39]. Previous studies done by other researchers proves that the pyrolysis process done in a vacuum condition provides a product with higher pores due to the higher interaction between char and compared to the typical nitrogen atmospheric pyrolysis process [40]. Furthermore, the sonication process which was carried out with the presence of HNO_3 and $KMnO_4$ also played a major role in the development of pores on the surface of magnetic biochar [41]. Therefore, the sonication process which was done in the presence of acidic and alkaline condition leads to fixation of a high amount of oxygen functionalities on the magnetic biochar's surface along with the partial destruction or degradation of its porous structure. This statement acknowledges the employment of HNO_3 and $KMnO_4$ on the production of magnetic biochar with higher BET surface area. Moreover, the white particles which are formed on the surface of magnetic biochar as shown in Fig. 3 are related to the attachment of iron particles on the surface of magnetic biochar [42].

The morphologies of the polymer composite along with the attachment of PANI particle on the surface of magnetic biochar are shown in Fig. 4. The in-situ polymerization process which was done for the preparation of a conductive polymer composites successfully attach PANI particles on the different type of pores on the surface of magnetic biochar. As can be seen from Fig. 4 at different magnification of FESEM images, tiny white particles of PANI were seen on the surface of magnetic biochar, in which the surface micropores and macropores of magnetic biochar in the composite disappear due to the occupying of external PANI particles. These images indicate that the in-situ polymerization process done can improve the dispersion of PANI particles in magnetic biochar and promote the electrolyte access and ion diffusion during the charge-discharge process for the specific conductivity measurement. Besides that, FESEM images from Fig. 4(e, f) demonstrate a higher number of PANI particles attachment on the surface of MBC, indicates the higher BET surface area possessed by MBC. These attachments would provide a higher electrical conductivity value compared MBOA and MBSA. In additional to that, these attachments would lead to higher ion diffusion during the charge-discharge process, leading to higher specific capacitance values. A similar type of studies which were done by other researchers acknowledge the success of in-situ polymerization on attachments of polymer particles on the surface of magnetic biochar for a better electrochemical performance [30].

3.1.2. X-ray diffractometry (XRD) analysis

The crystallinity and ferromagnetic phase presence in the magnetic biochar along with its attachment of PANI were investigated by the employment of XRD analysis. The results obtained from this analysis were compared with standard reference patterns and measurement to identify the ferromagnetic's phase of the MBO, MBS, and MBC [43]. The XRD patterns of the produced MBO, MBS and MBC are shown in Fig. 5 respectively. The major peaks were identified in X-ray diffraction were 35.48°, 57.72° and 63.22°. These peaks were identified as in the index plane such as 311, 511 and 106 of magnetite. The peaks corresponds to 111, which is crystal phase of FeO and the peaks 311 referred to α-iron structure. The carbide peaks are more intense for higher iron ratios in the precursor powder. These results are good agreement with previous researcher's [44] .Thus, the ferromagnetic phase of MBO and MBS are hematite (α-Fe_2O_3) while MBC exhibited a magnetite (Fe_3O_4) phase. The standard 2θ values and relative intensity for hematite [45] and magnetite [46] which were used for comparison acknowledge the presence of this phase. The sharp peaks and the position of main diffraction peaks of these samples indicate the well-crystalline structure of MBO, MBS, and MBC. This study highlights the employment of vacuum condition in a muffle furnace along with a high pyrolysis time and temperature leads to the production of novel MBC with a magnetite (Fe_3O_4) phase which is generally achieved by the co-precipitation route in the presence of Fe^{2+}/Fe^{3+} ions [47–49]. Besides that, the study done by Du et al. [50]

Please cite this article in press as: K.R. Thines, et al., A new route of magnetic biochar based polyaniline composites for supercapacitor electrode materials, J. Anal. Appl. Pyrol. (2016), http://dx.doi.org/10.1016/j.jaap.2016.08.004

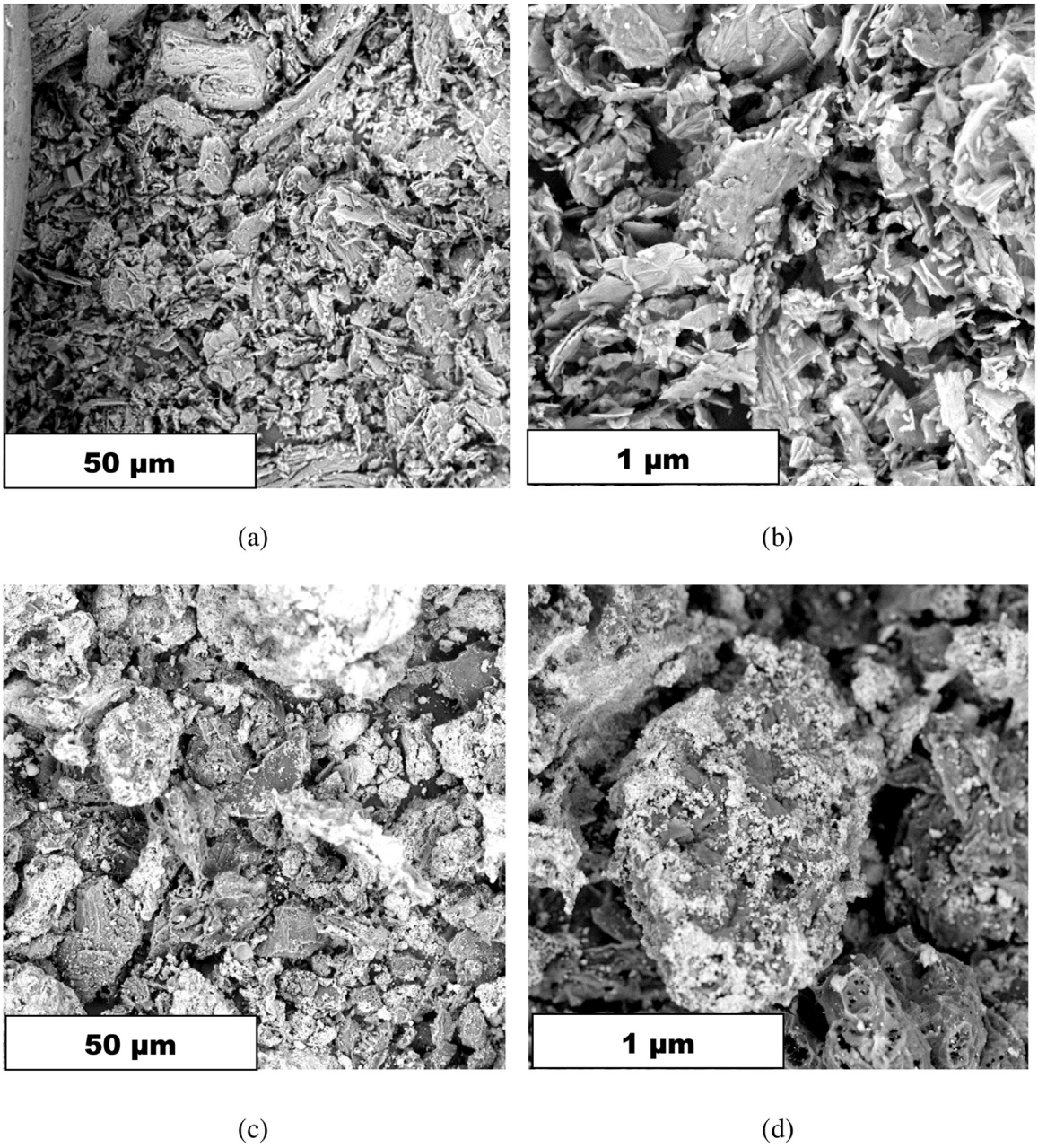

Fig. 2. FESEM images of (a, b) raw durian's rind (c, d) biochar at different magnification.

which highlights the development of magnetite-based magnetic biochar by the employment of the flow of inert gas such as argon during the annealing process provides an additional information for this research's outcome.

On the contrary, the identification of attachment of PANI particles on the surface of magnetic biochar could be analysis through as XRD as well. In general, broad peaks at $2\theta = 20.4^\circ$ and 25.1° indicate the present of the crystalline structure of PANI [51]. On that note, Fig. 6 demonstrates that all three MBOA, MBSA and MBCA polymer composite exhibited a broad peak at $2\theta = 20.4^\circ$ and 25.1° while maintaining the balance peaks which is associated with hematite and magnetite respectively, concluding that the crystalline structure of PANI is not affected by the loading of magnetic biochar due to well dispersion of magnetic biochar in the polymer matrix. Hence, result obtained from this analysis acknowledge the successful and novel attachment of hematite and magnetite from magnetic biochar into a polymer matrix as the previous study was done by other researchers only highlights the attachment of hematite and magnetite from a metallic salt or magnetic material into the PANI polymer matrix [52,53]. The stability of magnetic biochar depends on the pH, therefore play a vital role in stability of magnetic biochar on the surface of biochar. This could be magnetite to stable passivating film act as protection by choosing particular pH. The iron ions precipitate in the form of magnetite entering in to the solution. Therefore the nucleation and crystal growth follow the solution along the magnetite is super saturated in the form of Fe^2 and Fe ions.

3.1.3. Brunauer, Emmett and Teller (BET) surface area analysis

The specific surface area along with the N_2 adsorption isotherm behavior of MBO, MBS and MBC was determined by the BET method as these values are considered highly important due to the domination of surface properties in the interfacial behavior during the application in a conductive polymer. The values of BET surface

Please cite this article in press as: K.R. Thines, et al., A new route of magnetic biochar based polyaniline composites for supercapacitor electrode materials, J. Anal. Appl. Pyrol. (2016), http://dx.doi.org/10.1016/j.jaap.2016.08.004

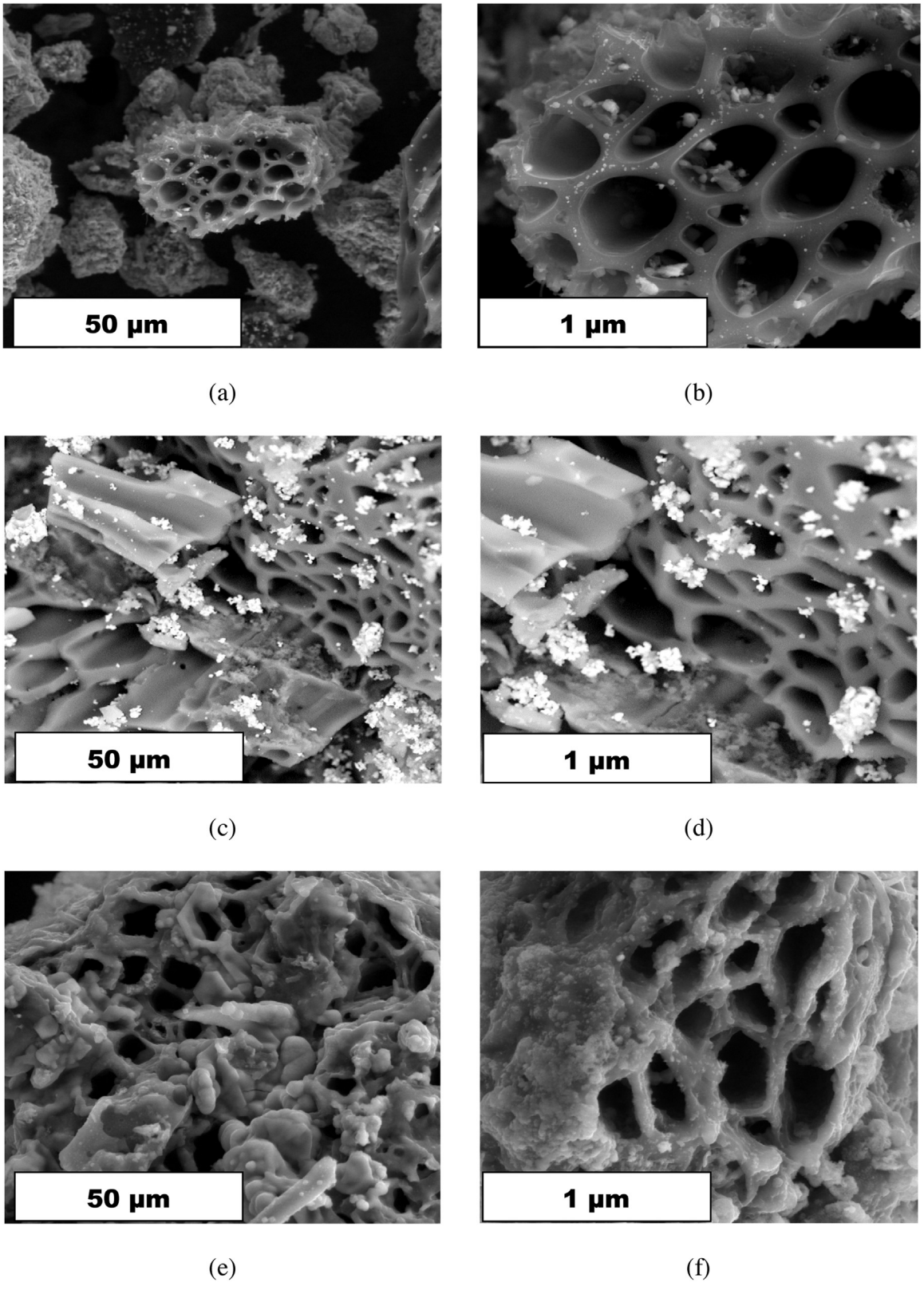

Fig. 3. FESEM images of (a, b) MBO (c, d) MBS and (e, f) MBC at different magnification.

area, total pore volume and pore width of MBO, MBS and MBC are demonstrated in Table 1. As can be seen from Table 1, an increase in the BET surface area and total pore volume led to a reduction in the size of pore width as done previously by other researchers [54]. Furthermore, Table 1 also demonstrates that the BET surface area and total pore volume increased after the deposition of iron, Fe ions in the biochar due to the decomposition of the oxygen functional groups during the pyrolysis process in the muffle furnace with a vacuum condition [55,56]. Furthermore, the reduction of Fe metal species during the pyrolysis process leads to an increase in the pore

Please cite this article in press as: K.R. Thines, et al., A new route of magnetic biochar based polyaniline composites for supercapacitor electrode materials, J. Anal. Appl. Pyrol. (2016), http://dx.doi.org/10.1016/j.jaap.2016.08.004

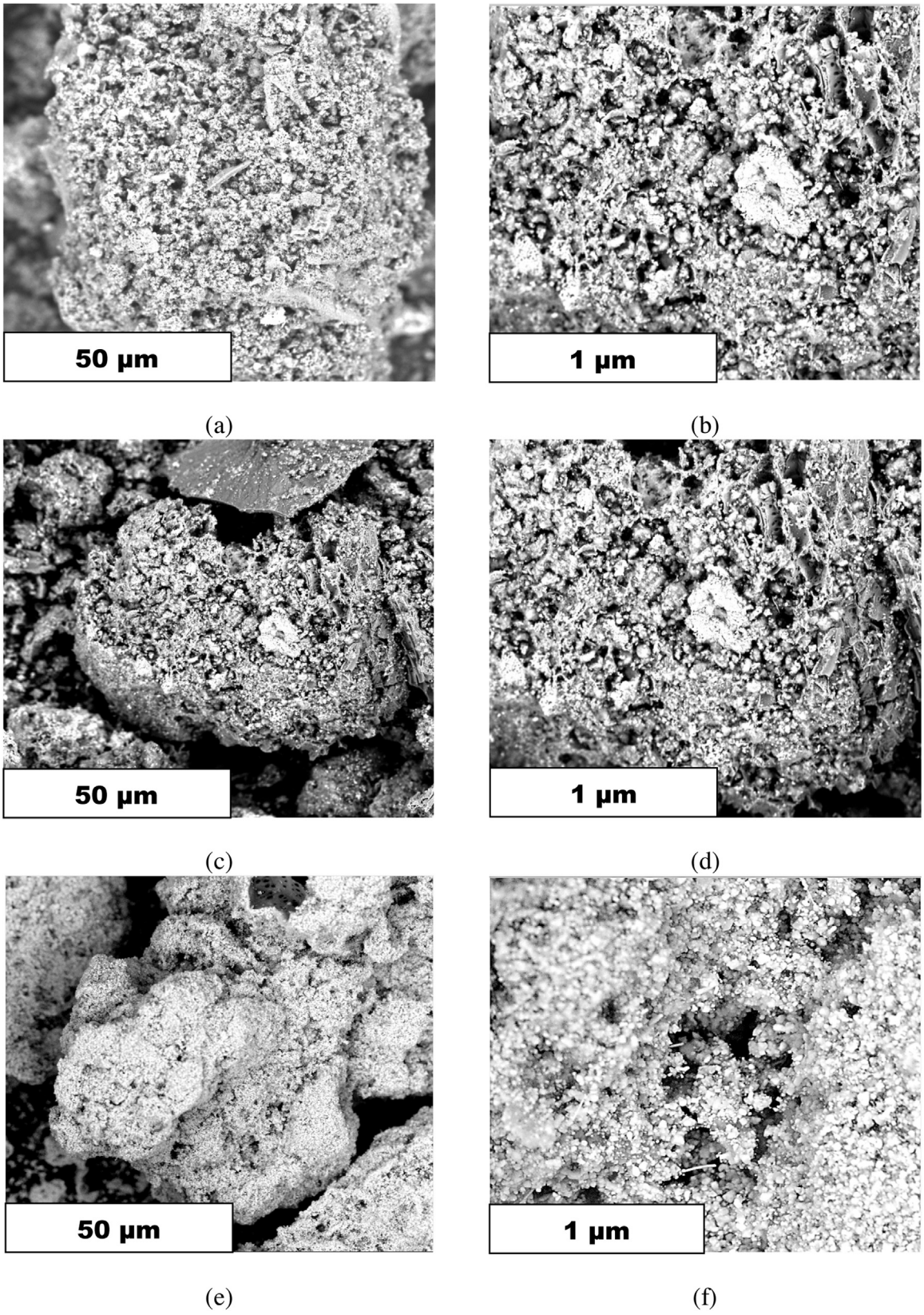

Fig. 4. FESEM images of (a, b) MBOA (c, d) MBSA (e, f) MBCA at different magnification.

volume due to carbon gasification, as agreed by other research work as well [57]. In additional, the N_2 adsorption or desorption isotherm of MBO, MBS and MBC is demonstrated in Fig. 7 in which all three magnetic biochar exhibited an adsorption isotherm of combination of type I (initial part of the plot is concave to the relative pressure (P/P_o) axis) and type IV isotherm (the hysteresis loop at the end of the plot). According to the IUPAC classification, Type I adsorption isotherm acknowledge the availability of pores in micropores

Please cite this article in press as: K.R. Thines, et al., A new route of magnetic biochar based polyaniline composites for supercapacitor electrode materials, J. Anal. Appl. Pyrol. (2016), http://dx.doi.org/10.1016/j.jaap.2016.08.004

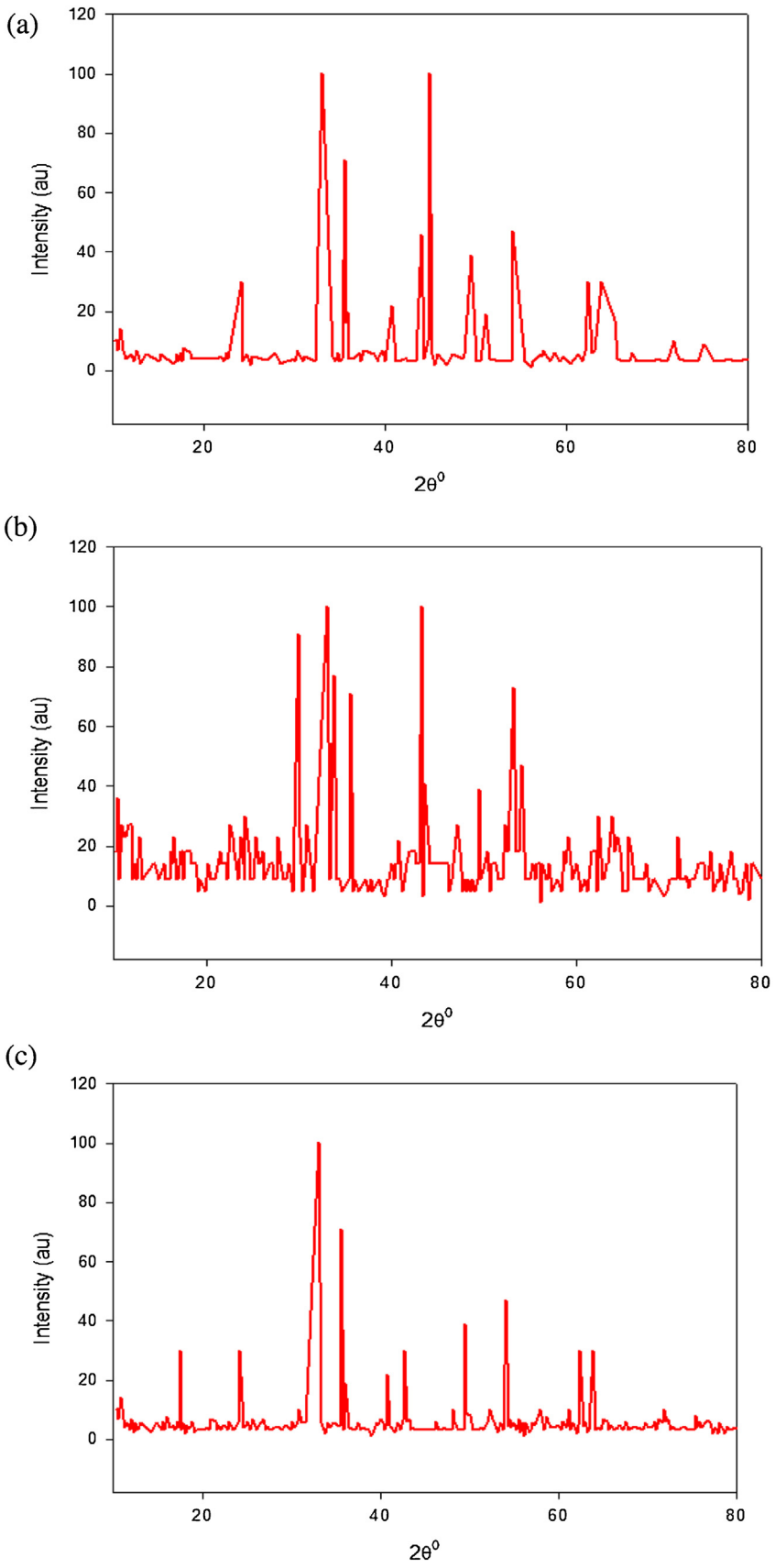

Fig. 5. XRD Analysis of (a) MBO (b) MBS and (c) MBC.

Please cite this article in press as: K.R. Thines, et al., A new route of magnetic biochar based polyaniline composites for supercapacitor electrode materials, J. Anal. Appl. Pyrol. (2016), http://dx.doi.org/10.1016/j.jaap.2016.08.004

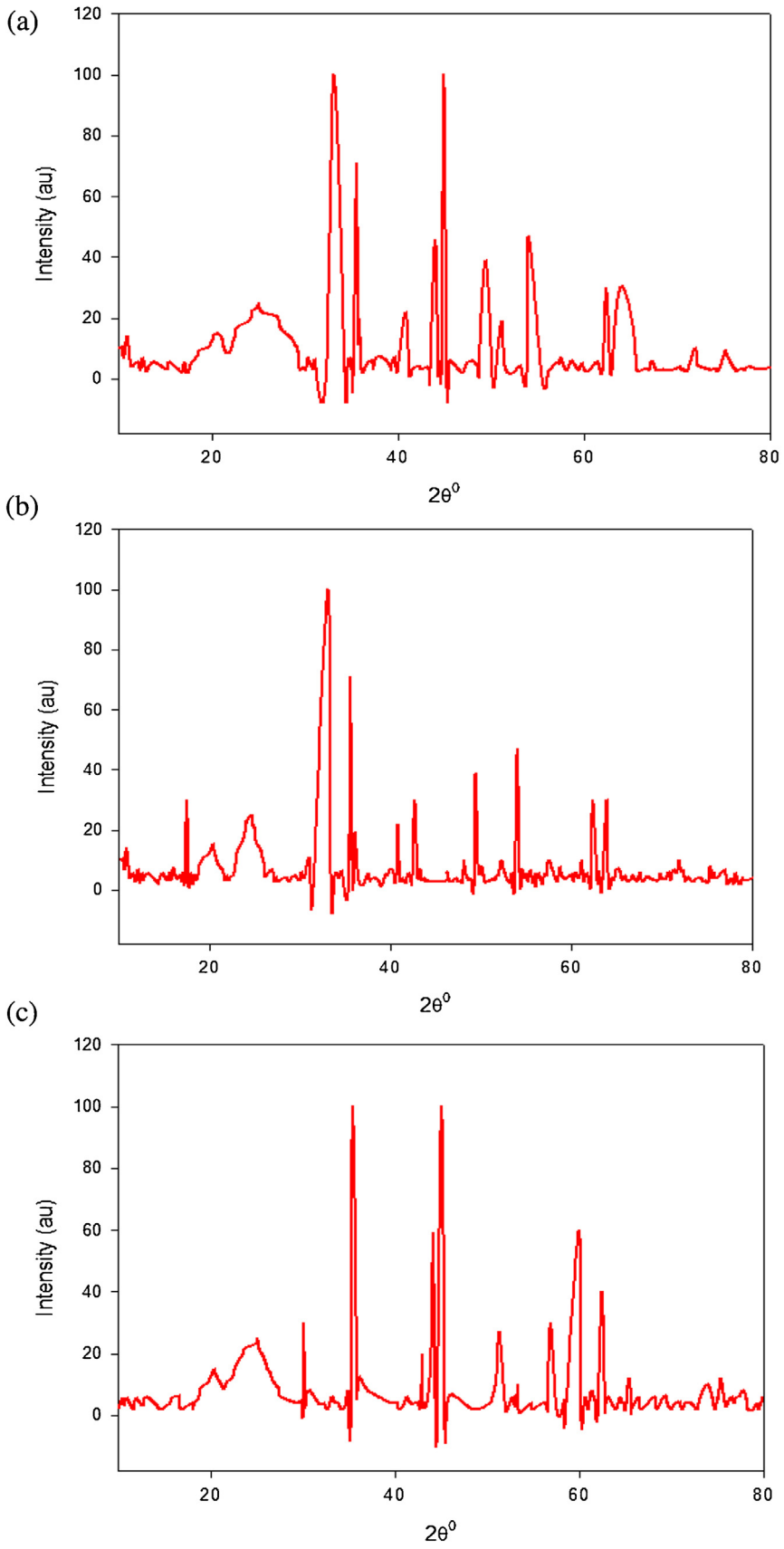

Fig. 6. XRD analysis of (a) MBOA (b) MBSA and (c) MBCA.

Please cite this article in press as: K.R. Thines, et al., A new route of magnetic biochar based polyaniline composites for supercapacitor electrode materials, J. Anal. Appl. Pyrol. (2016), http://dx.doi.org/10.1016/j.jaap.2016.08.004

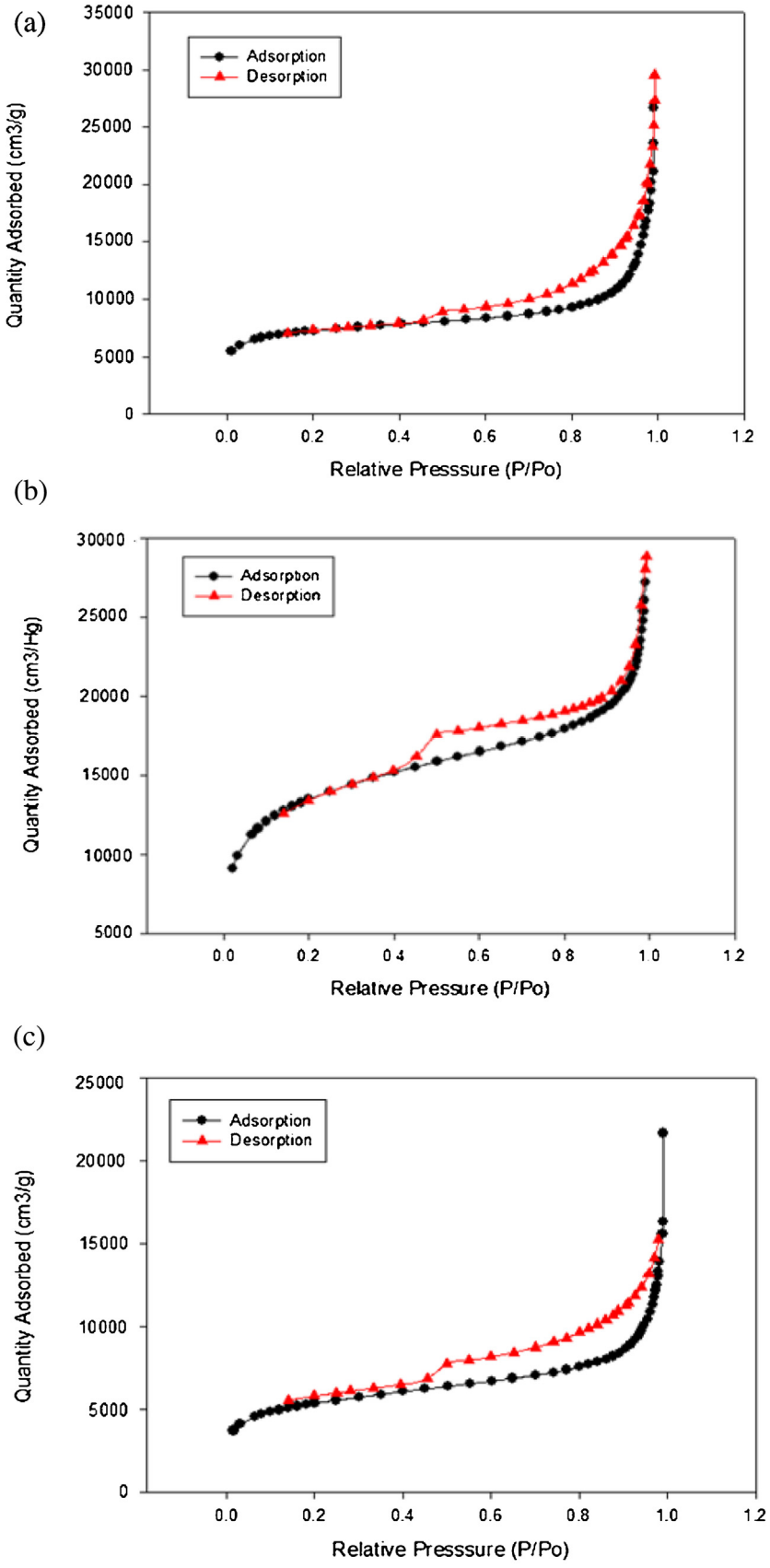

Fig. 7. N_2 adsorption/desorption isotherm of (a) MBO (b) MBS and (c) MBC.

Please cite this article in press as: K.R. Thines, et al., A new route of magnetic biochar based polyaniline composites for supercapacitor electrode materials, J. Anal. Appl. Pyrol. (2016), http://dx.doi.org/10.1016/j.jaap.2016.08.004

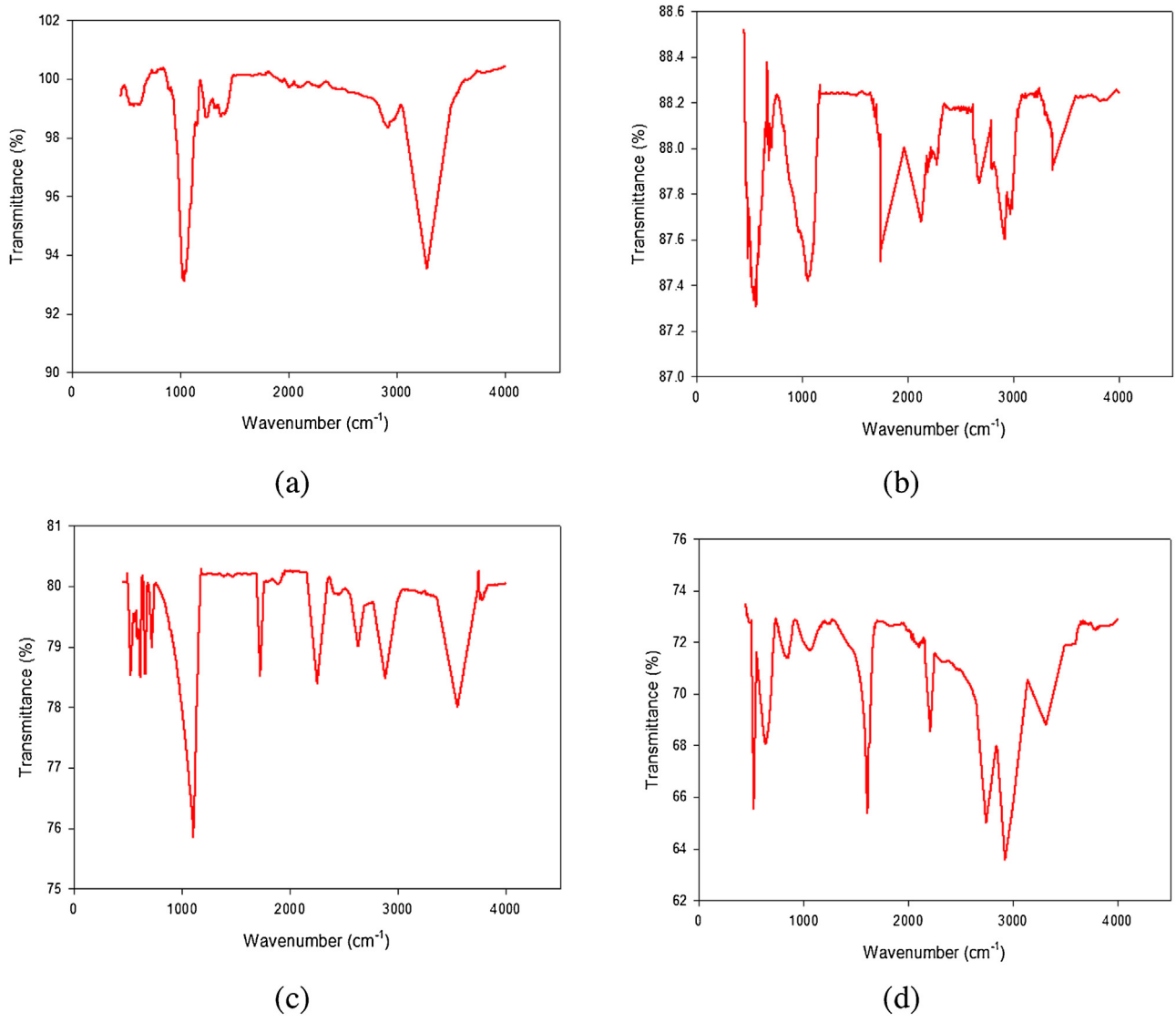

Fig. 8. FTIR images of (a) Raw durian's rind (b) MBO (c) MBS and (d) MBC.

Table 1
Main Characteristics of MBO, MBS and MBC.

Sample	Main characteristics		
	BET surface area (m^2/g)	Total pore volume (cm^3/g)	Pore width (nm)
Durian's rind	10.34	0.00219	0.0308
MBO	830	0.722	2.47
MBS	827	0.511	2.17
MBC	835	0.497	3.11

condition along with the exposed surface residing inside the micropores. On the other hand, the Type IV isotherm acknowledges the present of small mesopores and the capillary condensation of mesopores and macropores through the hysteresis loop [58]. The similar type of result was encountered by other researchers during the deposition of metal in the biochar as well [59,60]. The BET surface area of magnetic biochar – polymer composite is discussed later in the specific capacitance, C_S section.

3.1.4. Fourier transform infrared spectroscopy (FTIR) analysis

The raw durian's rind along with MBO, MBS and MBC was further characterized by FTIR to determine the presence of specific particular bands which relates to certain functional groups. As can be seen from Fig. 8, raw durian's rind exhibited peaks at different wavenumber compared with magnetic biochar in which all three MBO, MBS and MBC exhibited a similar type of spectrum at a similar range of wavenumber. Based on Fig. 8(a), raw durian's rind exhibited a broad and sharp peak at 3200–3500 cm^{-1} which correspond to the O—H stretching vibration of OH group in cellulose molecules along with the intramolecular and intermolecular hydrogen bonds. This narrower and high-intensity peaks confirms the high cellulose content of durian's rind [61,62]. Moreover, the FTIR spectrum exhibited a peak of 1030 cm^{-1} which indicates the C—O stretching vibration of the acetyl group of lignin [63] in raw durian's rind [63]. Furthermore, the FTIR spectrum of raw durian's rind also exhibited a peak of 1371 cm^{-1} which corresponds to the C—H stretching of cellulose in the durian's rind [64]. All the peaks present in the raw durian's rind indicated that it contains a high level of cellulose which will be converted into various functional groups during the sonication process with HNO_3 and $KMnO_4$ along with the respected metallic salt.

Likewise, the FTIR spectrum of MBO, MBS and MBC are demonstrated in Fig. 8(b)–(d) respectively. In general, all three type of magnetic biochar demonstrated almost similar peaks due to the

Please cite this article in press as: K.R. Thines, et al., A new route of magnetic biochar based polyaniline composites for supercapacitor electrode materials, J. Anal. Appl. Pyrol. (2016), http://dx.doi.org/10.1016/j.jaap.2016.08.004

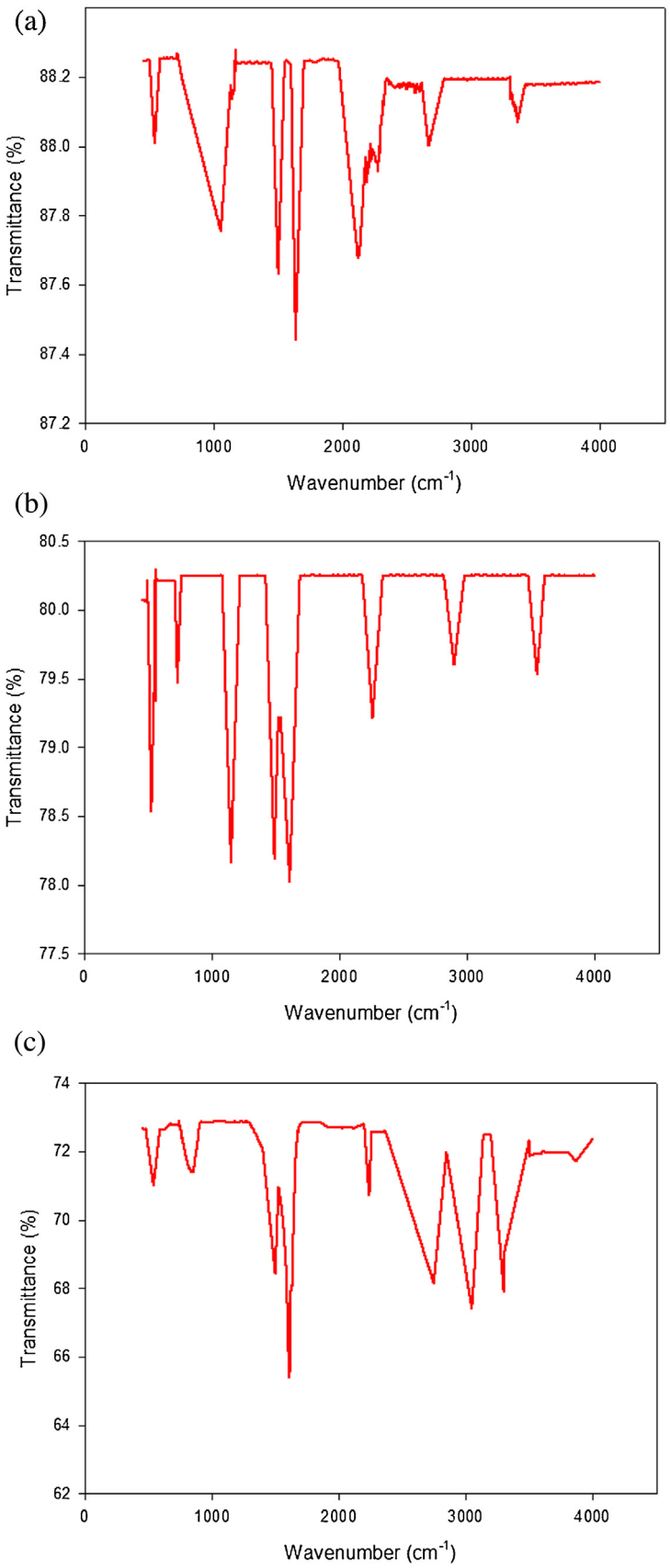

Fig. 9. FTIR images of (a) MBOA (b) MBSA (c) MBCA.

Table 2
Summary of FTIR Spectrum of MBO, MBS and MBC.

MBO band position (cm^{-1})	MBS band position (cm^{-1})	MBC band position (cm^{-1})	Possible assignments	Reference
3374	3553	3317	O—H stretching, free hydroxyl	[90]
2910	2879	2925	C—H stretching (alkenes)	[91]
2671	2627	2743	H—C=O: C—H stretching (aldehydes)	[92]
2130	2254	2214	—C≡C— stretching (alkynes)	[93]
1747	1726	1611	C=O stretching (carboxylic acids)	[94]
1055	1104	1087	C—N stretching (aliphatic amines)	[95]
685	662	636	=C—H bending (alkenes)	[96]

HNO_3 and $KMnO_4$ solution used in the presence of iron ion based salt during the sonication process. All three type of magnetic biochar exhibited a similar peak at 500–550 cm^{-1} which correspond to the presence of iron oxide in the optimized magnetic biochar. Apart from that, MBS exhibited a sharp peak at 726 cm^{-1} which correspond to the C-S stretching vibration in the magnetic biochar due to the employment of $FeSO_4{\cdot}7H_2O$ as the metallic salt [65]. Likewise, MBC exhibited a short sharp peak at 824 cm^{-1} which correspond to the C—Cl stretching vibration in the magnetic biochar due to the employment of $FeCl_3{\cdot}6H_2O$ as the metallic salt [66]. On the other hand, the main purpose of the sonication process done prior the pyrolysis process would be to enhance the formation of pores along with the attachment of functional groups on the surface of magnetic biochar during the decomposition of surface volatile substance. The presence of functional groups in MBO, MBS and MBC were found to be in the similar FTIR spectrum as demonstrated in Table 2. Furthermore, few notable research works which produced the similar type of FTIR spectrum were acknowledged in Table 2 as well. As can be seen from Table 2, the FTIR spectrum which corresponds to the presence of C—N and C=O stretching acknowledge the utilization of HNO_3 during the sonication process while other FTIR spectrum acknowledges the formation of the different functional group on the surface of magnetic biochar. Apart from that, the FTIR peaks related to O—H stretching for all three magnetic biochar were found to be shorter compared to raw durian's rind, indicating the transformation of cellulose material into magnetized carbon material. The overall FTIR spectrum of optimized magnetic biochar acknowledges the formation of magnetic biochar with high BET surface area with the additional of the important functional group on the surface of magnetic biochar for further application purpose. On the contrary, Fig. 9 exhibits the FTIR spectrum to further confirm the attachment of PANI particles on the surface of magnetic biochar.

As can be seen from Fig. 9(a)–(c), the FTIR spectrum exhibited peaks of 1635, 1570, 1610 [67] and 1500, 1440, 1500 cm^{-1} [68] which indicates the C=C stretching of quinonoid ring and benzenoid ring of PANI respectively. Furthermore, the C—N stretching of secondary aromatic amine (1050, 740, 852) and the aromatic C—H stretching (2671, 3050, 2747) of PANI also can be seen in Fig. 9(a)–(c) respectively. The appearance of these peaks further confirms the presence of PANI in the composites [69,70]. However, certain peaks which were found in magnetic biochar such as the O—H stretching and C—H stretching (carboxyl) retained its peaks in the composite as well with a higher wavenumber for PANI polymer composite. A similar type of result was encountered by other researchers during the incorporation of hematite or magnetite-based material into PANI chain [71–73].

3.1.5. UV–vis spectroscopy analysis

The UV–vis spectroscopy analysis was employed to characterize the interfacial interaction between the polymer such as PANI with magnetic biochar particles such as MBO, MBS, and MBC. Besides that, the absorption peaks at respective wavelength can be used to determine the electron transition occurs between the magnetic biochar and polymer chain. Generally, a typical absorption spectrum of PANI dispersions has two distinct absorption peaks at about 330 and 640 nm as shown in Fig. 10. This absorption peak is generally attributed to the $\pi-\pi^*$ transition of the benzenoid rind and the π-polaron benzenoid-quinoid excitonic transition respectively [74]. These peaks were found to be identical to conventional PANI powders as done by other researchers [75,76]. On the other hand, Fig. 10 demonstrates that the two distinct absorption peaks have been shifted at about 360 and 725 nm with a weaken characterization absorption peaks with respect to MBO and MBS. The shift from 640 to 725 nm is generally referred as a polaronic transition which arises due to the interaction of hematite structure in MBO and MBS with the PANI ring while the shift from 330 to 360 nm is attributed to the bathochromic shift due to the introduction of hematite structure into PANI's chain. A similar study was done by Dallas et al. [77], Singh et al. [73], and Yan et al. [78] exhibited the almost similar type of absorption peaks for both PANI and hematite loaded PANI structure. However, the absorption peak for MBCA exhibited a shift from 330 to 315 nm and 640–570 nm indicates the interaction between the magnetite phases in MBC with the PANI chain while the absorption peak at 390 nm corresponds to the presence of polaron–π^* transition in the MBC-PANI structure. The presence of this extra transition explains the possibility to achieve a high electrical conductivity value compared to MBOA and MBSA composite due to the increase in charge mobility in the composite. On that note, a similar study was done by Lu et al. [74] and Kong et al. [79] exhibited a similar type of absorption peaks for the magnetite-loaded PANI structure.

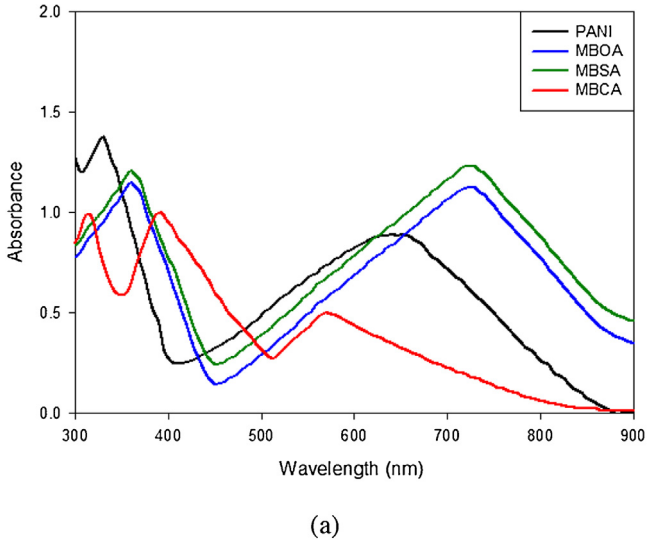

Fig. 10. UV–vis spectrums of PANI, MBOA, MBSA, and MBCA.

3.2. Electrical conductivity of magnetic biochar – PANI composite

The weight of magnetic biochar and aniline monomer was all manipulated to study its effect on the electrical conductivity of the conductive polymer composite produced. Fig. 11 demonstrates

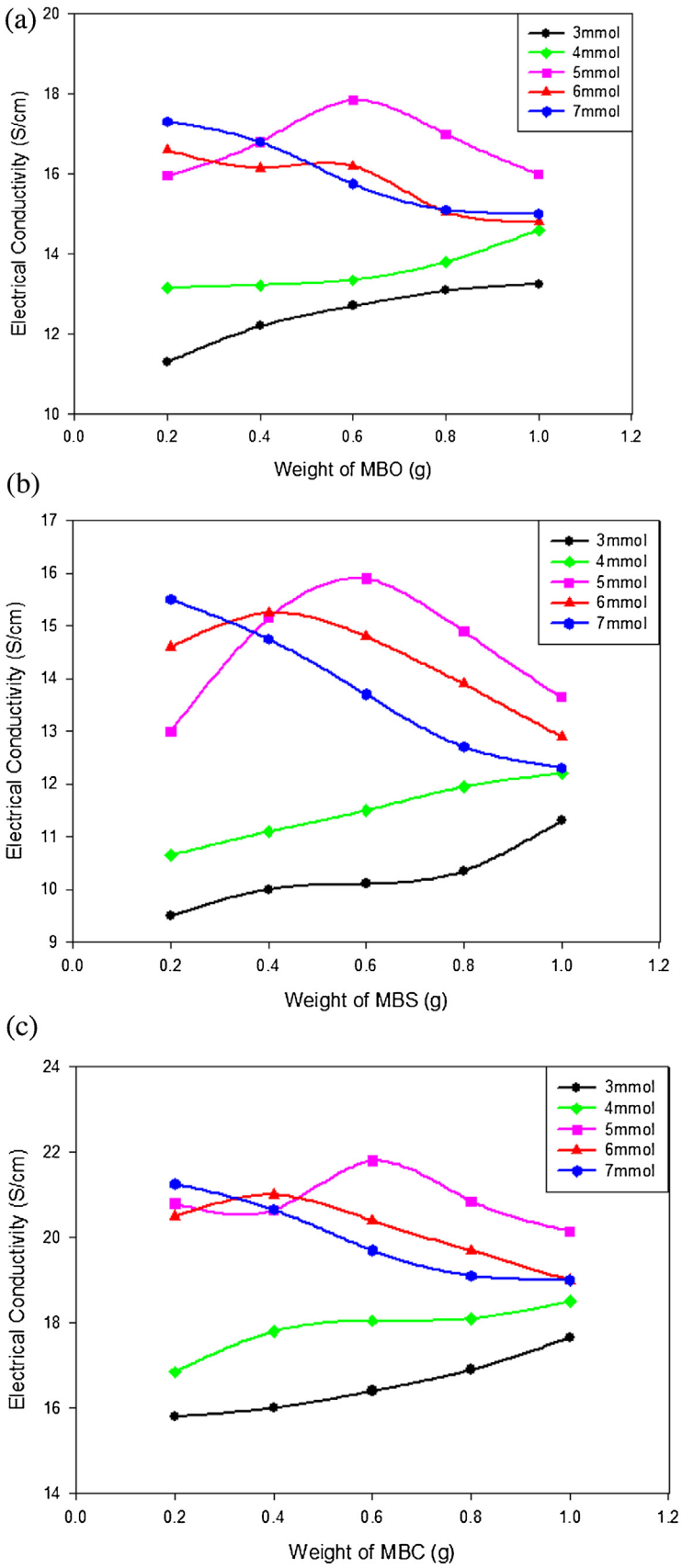

Fig. 11. Electrical conductivity of (a) MBOA composite (b) MBSA composite (c) MBCA composite.

the trend of electrical conductivity of MBOA, MBSA, and MBCA respectively. The electrical conductivity of the magnetic biochar doped polymer indicates that the dopant does not block the flow of electric current in the polymer matrix to a significant extent. As can be seen, the electrical conductivity of the MBOA, MBSA, and MBCA composite was found to increase gradually for both 3 mmol and 4 mmol of aniline monomer as the weight of magnetic biochar increases. This would be due to the availability of sufficient mobile charge carriers from magnetic biochar to conduct electricity in the PANI chain. As the weight of aniline monomer increased to 5 mmol, the electrical conductivity gradually increased as the weight of magnetic biochar increases from 0.2 to 0.6 g and then slowly decreases as the weight of magnetic biochar reaches 1.0 g. As the weight of aniline monomer increases beyond 5 mmol, the electrical conductivity was found to reduce gradually as the weight of magnetic biochar increases. This trend of electrical conductivity proves that the weight of magnetic biochar along with aniline monomer plays a vital role in the production of magnetic biochar – polymer composite with high electrical conductivity. As the content of aniline monomer increases beyond the weight of magnetic biochar, the particles tend to block the macropores and micropores of the magnetic biochar, leading to a reduction in the availability of surface area for the transport of mobile charge carriers during the conductivity test. On the other hand, an excessive amount of magnetic biochar reduces the electrical conductivity due to the lower electrical conductivity of magnetic biochar. On that note, the doping of conductive polymer generally refers to charge transfer and the associated insertion of a counter ion. A doping process introduces mobile charge carriers into the conjugated??-electronic matrix of conductive polymer which leads to an increase in the electrical conductivity. At a lower doping level, these mobile charge carriers are self-localized and accumulate to from nonlinear configurations in which the transport of mobile carriers occurs along the conjugated chains. As for high dopant level, the transports of mobile charge carries are found to be delocalized along the polymer chain [80–82]. In additional to that, as the doping content increases, the volume of the sample increases, leading to a reduction in the conductivity values as well due to the reduction in the number of electron transfer per unit volume, which results in two contrary effects on the conductivity of conductive polymer's composite. The conductivity value also were found to increases as the dopant due to the increase in polarizability of the carrier solvents [83]. Furthermore, Fig. 11 demonstrates that the highest electrical conductivity obtained for MBOA, MBSA, and MBCA composite were 17.85, 15.90, and 21.80 S/cm respectively. The electrical conductivity of all these composites were found to be within the same range due to mobile charge presents based on the composition of these magnetic biochar. The electrical conductivity of PANI was measured to be 4 S/cm respectively, indicating a remarkable increase of electrical conductivity in the magnetic biochar – polymer composite produced. The results obtained from XRD analysis previously demonstrated that the ferromagnetic phase of MBO and MBS were hematite while MBC possessed the magnetite phase. These almost similar ferromagnetic phases played a vital role in the production of conductive polymer within the same range of electrical conductivity. On the other hand, MBCA exhibited a slightly higher electrical conductivity compared with other conductive polymer composite due to the high BET surface area of MBC as stated in Table 1.

3.3. Electrochemical performance of magnetic biochar and polymer composite

3.3.1. Cyclic voltammograms (CV) curve of magnetic biochar – polymer composite

The CV curve method was employed to evaluate the performance and capacitance behavior of the prepared magnetic biochar and its respective polymer composite along with its capacitance value to determine its suitability as an electrode in supercapacitor as shown in Figs. 12 and 13. The CV curves which at different scan rates exhibited that these two figures indicates the obvious capacitive nature of the fabricated electrode of MBO, MBS, MBC, MBOA, MBSA, and MBCA. On that note, the voltammograms of magnetic biochar and its PANI composite from Figs. 12 and 13 exhibited a fairly broad and rectangular in shape without the presence of any sharp current peaks. This characterization of the voltammograms is considered to be the primary characteristics of a capacitor material [84]. However, the slight deviation of the CV shapes from the ideal rectangular shape is due to the polarization of the magnetic biochar and polymer composite [85]. On that note, the quasi-rectangular shape exhibited by the magnetic biochar and polymer composite indicates the significant contribution from electrical double layer capacitance (EDLC). Similarly, all voltammetric curves exhibited symmetrical negative sweeps to their positive counterparts indicating an excellent reversibility in the high positive potential range.

Based on Figs. 12 (d) and 13 (d), MBC and MBCA which exhibited a more visible bending in the CV curves implies a strong pseudocapacitive feature. All the CV curves from Fig. 12 and 13 exhibited a higher current density at the higher scan rate. A larger CV curve area generally leads to a higher specific capacitance, C_s value [12,86]. Hence, by referring to Figs. 12 (d) and 13 (d), MBC and MBCA exhibited a larger curve area, leading to a higher specific capacitance value compared to other magnetic biochar and polymer composite. On that note, MBC and MBCA exhibited a slightly better electrochemical performance compared to MBO, MBS, MBOA and MBSA most probably due to the higher BET surface area value which enhances electron transfer and mobility of charge carriers. However, the extraordinary characteristics of MBO, MBS and MBC such as high surface area, good pore volume, and the presence of micropores, mesopores and macropores contributed the most to a significant electrochemical performance of the prepared polymer composite to fall within the same range. On the other hand, polymer composite of PANI-based on MBO, MBS and MBC exhibited a better electrochemical performance compared to magnetic biochar due to the availability of both magnetic biochar and polymer contributing to the capacitance value. Besides that, the formation of PANI particles on the porous surface of magnetic biochar was well dispersed, which leads to the opening of more active sites for the accessibility of pseudocapacitance to the electrolyte ions, leading to a higher utilization of active materials for electrochemical reactions [30]. The BET surface area value of the prepared polymer composite value are demonstrated in Table 3, in which the polymer composite exhibited a lower BET surface area value compared to its parent magnetic biochar, indicating the successful formation of PANI particles on the surface of MBO, MBS and MBC respectively.

Table 3
Physical and Capacitive Properties of Magnetic Biochar and Polymer Composite.

Sample	BET surface area (m^2/g)	C_S at 10 mV/s (F/g)	Energy density at 10 mV/s (Wh/kg)
MBO	830.00	150	18.75
MBS	827.00	115	14.36
MBC	835.00	180	22.50
PANI	286.38	345	43.13
MBOA	501.32	530	66.25
MBSA	505.61	425	53.13
MBCA	510.50	615	76.88

3.3.2. Specific capacitance, C_S and energy density of magnetic biochar – polymer composite

The C_S value of the magnetic biochar – polymer composite which was fabricated as electrode could be determined from the CV curve as well. As can be seen, from Fig. 13, the C_S value was found to

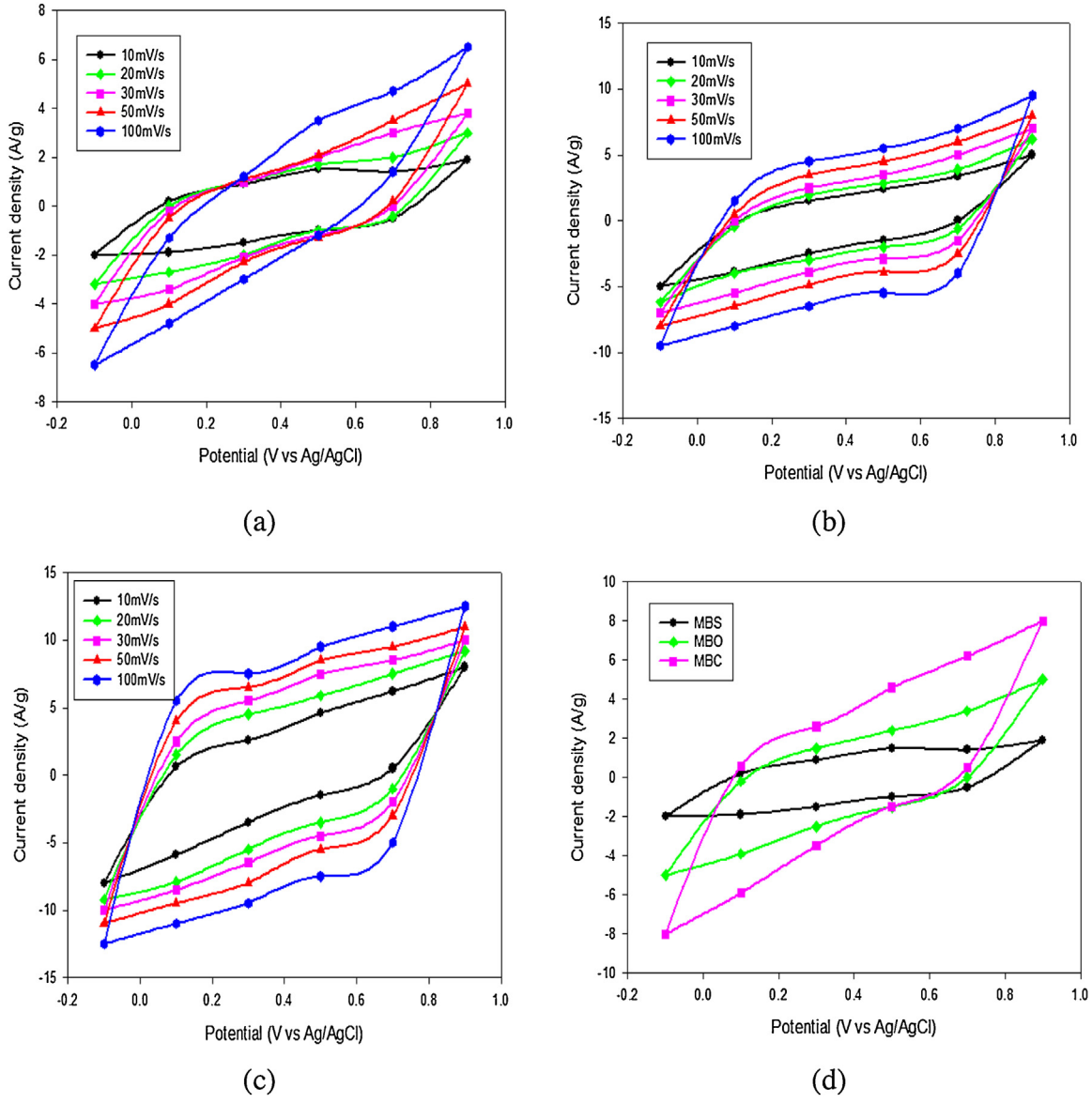

Fig. 12. CV curves of (a) MBO (b) MBS (c) MBC (d) Comparison of CV curve of MBO, MBS and MBC at the scan rate value 10 mV/s.

decrease as the scan rate increases due to more difficult penetration and diffusion of the electrolyte ions under higher scan rates [87,88]. Besides that, the C_S reduces at high scan rate due to the insufficient time for the ionic transportation restricts ion doping inside the PANI particles. It can be observed that the electrodes based on MBOA, MBSA and MBCA possess higher C_S value compared with the electrodes on their individual component (MBO, MBS, MBC, and PANI). As demonstrated by Fig. 13, MBCA exhibited the highest C_S value of 615, 580, 545, 475, and 400 F/g at respective scan rates of 10, 20, 30, 50 and 100 mV/s. The overall C_S value of magnetic biochar and polymer composite is demonstrated in Table 3. These results acknowledge on the improvement done on the electrical conductivity and C_s of PANI by co-operating with magnetic biochar. These results also indicate that the high BET surface area value of MBC plays a vital role on the electrochemical performance of polymer composite prepared based on it. Furthermore, the energy density value of magnetic biochar and polymer composite as demonstrated in Table 3 indicates that the MBCA have the highest energy density value of 76.88 Wh/kg compared to other material. Energy density which is generally referred as the amount of energy can be stored in a capacitor per volume of that capacitor plays an important role in the determination of the electrochemical performance of magnetic biochar and polymer composite. An important parameter to obtain a high energy density value would be the high BET surface area and narrow pore size distribution of both magnetic biochar and polymer composite which favors the formation of a high amount of double layers and ease the transport of the electrolyte ions. Besides that, the well-dispersed PANI particles over the surface of magnetic biochar are able to prevent the agglomeration of particles in the polymer composite, leading to an enhanced electrical double layer capacitance to the overall specific capacitance value. These agglomerations also significantly shorten the diffusion and migration paths of electrolyte ions during the rapid charge/discharge process to increase the energy density of magnetic biochar and polymer composite [89]. The result from this study highlights the significant novel application of magnetic biochar as a dopant in a polymer composite which was then fabricated as an electrode for a high capacitance and energy density

Please cite this article in press as: K.R. Thines, et al., A new route of magnetic biochar based polyaniline composites for supercapacitor electrode materials, J. Anal. Appl. Pyrol. (2016), http://dx.doi.org/10.1016/j.jaap.2016.08.004

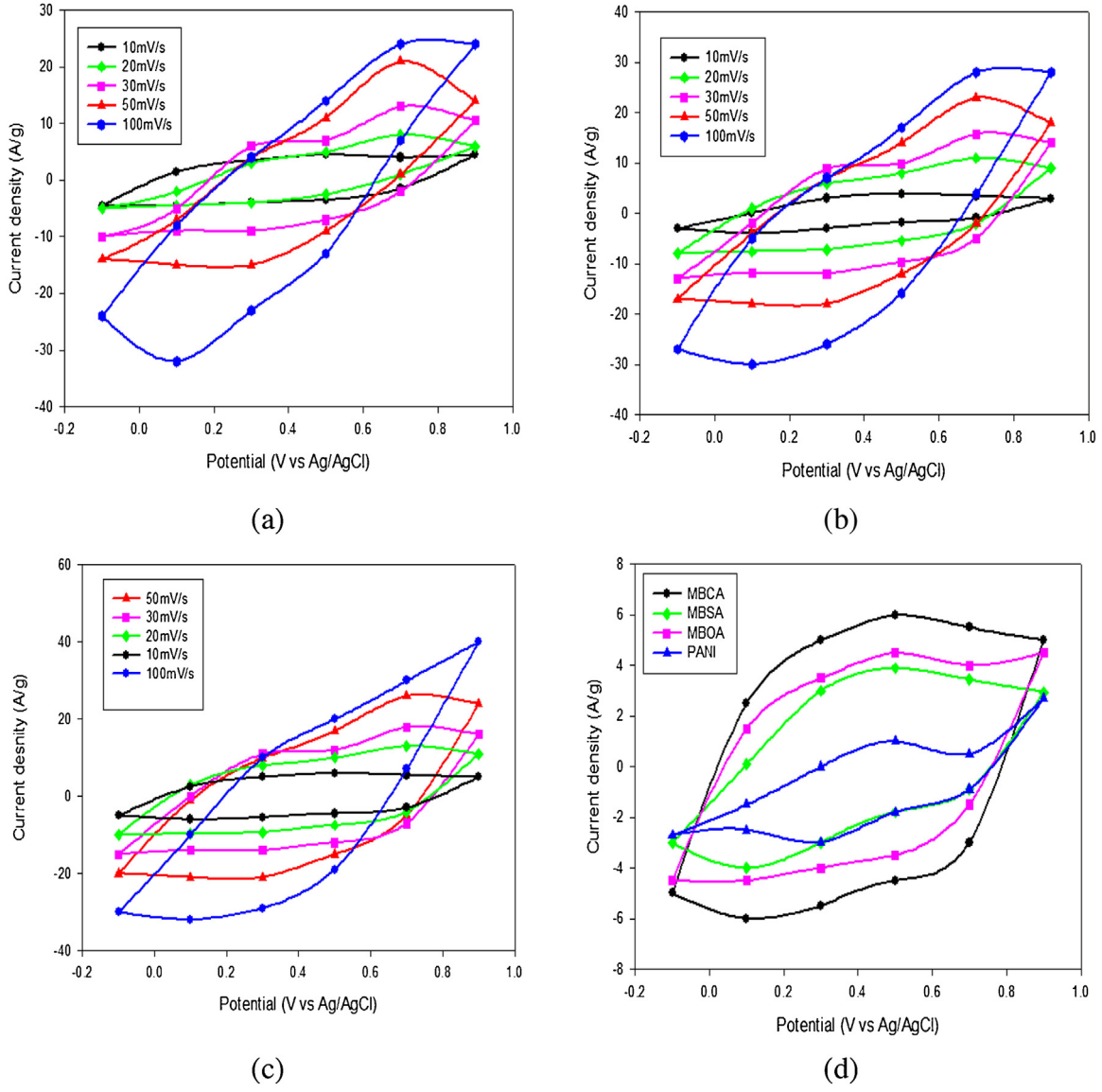

Fig. 13. CV curves of (a) MBOA (b) MBSA (c) MBCA (d) Comparison of CV curves of MBOA, MBSA, MBCA and PANI at the scan rate value 10 mV/s.

Table 4
Physical and Capacitive Properties of Magnetic Biochar and Polymer Composite.

Polymer composite	C_S (F/g)	Energy density (Wh/kg)	Reference
PANI/boron doped graphene	189	30.1	[88]
PANI coated stainless steel	453	0.357	[97]
PANI/Bamboo carbon composite	277	47.5	[98]
PANI coated boron doped biomass	421	45.2	[30]
PANI/reduced-graphene oxide/molybdenum oxide composite	553	28.6	[99]
PANI/SnO_2 composite	305.3	42.4	[100]
PANI/mesoporous carbon composite	87.4	23.8	[101]

value. The overall comparison of capacitance and energy density value obtained from this research with results obtained from the similar type of research is demonstrated in Table 4, justifying the significant result obtained from this research.

4. Conclusion

This study focused on the application of novel vacuum condition in an electrical muffle furnace for the production of magnetic biochar employing durian's rind as the raw material without the flow of carrier gas. Magnetic biochar impregnated with three different metallic salts were successfully produced with high porosity at a pyrolysis temperature and time of 800 °C and 25 min. This condition contributed to a high BET surface area value of 830, 827, and 835 m^2/g with respect to MBO, MBS, and MBC. This magnetic biochar was successfully employed to support and disperse PANI particles for the application of an electrode's material of a supercapacitor. The as-prepared MBOA, MBSA and MBCA composite exhibited an enhanced specific capacitance compared with the pure PANI and magnetic biochar due to the synergetic effect in the composite. The highest specific capacitance of 615 F/g at 10 mV/s and energy density of 76.88 Wh/kg were demonstrated by the MBCA composite, which is considered favorably high compared to the existing PANI coated carbon composites. This result suggests that the magnetic biochar – PANI composite can be employed

Please cite this article in press as: K.R. Thines, et al., A new route of magnetic biochar based polyaniline composites for supercapacitor electrode materials, J. Anal. Appl. Pyrol. (2016), http://dx.doi.org/10.1016/j.jaap.2016.08.004

as an effective electrode material candidate to produce low-cost supercapacitors. Furthermore, this study establishes a new route on the production of low-cost magnetized carbon-based polymer composite with high electrochemical activity.

References

[1] R. Kurzweil, The Singularity Is Near: When Humans Transcend Biology, Penguin p, 2005.
[2] J.S.C. Kilby, ChemPhysChem 2 (2001) 482.
[3] M.J. Comstock, Introduction to Microlithography, American Chemical Society, 1983, p. i.
[4] M.J. Comstock, M.J. Comstock, in: M.J. Comstock, M.J. Comstock (Eds.), Polymers for Microelectronics, American Chemical Society, 1993, 2016, p. i.
[5] R. Tummala, E.J. Rymaszewski, A.G. Klopfenstein, Microelectronics Packaging Handbook: Technology Drivers, Springer Science & Business Media, 2012.
[6] E. Donkor, A.K. Viswanath, S. Pearton, J. Lee, W.P. Gomes, X. Xiang, K. Leo, D. Lie, K. Wang, E. Zanoni, Handbook of Advanced Electronic and Photonic Materials and Devices Conducting Polymers, 2001.
[7] M.J. Comstock, Polymer Materials for Electronic Applications, American Chemical Society, 1982 (p. i.).
[8] A.S. Dunn, Polym. Int. 24 (1991) 256.
[9] M. Winter, R.J. Brodd, Chem. Rev. 104 (2004) 4245.
[10] H. Chen, D. Liu, Z. Shen, B. Bao, S. Zhao, L. Wu, Electrochim. Acta 180 (2015) 241.
[11] R.R. Salunkhe, Y.H. Lee, K.H. Chang, J.M. Li, P. Simon, J. Tang, N.L. Torad, C.C. Hu, Y. Yamauchi, Chem.—Eur. J. 20 (2014) 13838.
[12] H. Chen, S. Zhou, M. Chen, L. Wu, J. Mater. Chem. 22 (2012) 25207.
[13] H. Chen, L. Hu, Y. Yan, R. Che, M. Chen, L. Wu, Adv. Energy Mater. 3 (2013) 1636.
[14] H. Chen, L. Hu, M. Chen, Y. Yan, L. Wu, Adv. Funct. Mater. 24 (2014) 934.
[15] H. Jiang, J. Ma, C. Li, Adv. Mater. 24 (2012) 4197.
[16] K. Wang, H. Wu, Y. Meng, Z. Wei, Small 10 (2014) 14.
[17] G.A. Snook, P. Kao, A.S. Best, J. Power Sources 196 (2011) 1.
[18] Y. Atassi, M. Tally, M. Ismail, 0809, 3552, 2008.
[19] G. Wang, L. Zhang, J. Zhang, Chem. Soc. Rev. 41 (2012) 797.
[20] K. Zhang, L.L. Zhang, X. Zhao, J. Wu, Chem. Mater. 22 (2010) 1392.
[21] X. Zang, X. Li, M. Zhu, X. Li, Z. Zhen, Y. He, K. Wang, J. Wei, F. Kang, H. Zhu, Nanoscale 7 (2015) 7318.
[22] Y. Yan, Q. Cheng, Z. Zhu, V. Pavlínek, P. Sáha, C. Li, J. Power Sources 240 (2013) 544.
[23] H. Zengin, W. Zhou, J. Jin, R. Czerw, D.W. Smith, L. Echegoyen, D.L. Carroll, S.H. Foulger, J. Ballato, Adv. Mater. 14 (2002) 1480.
[24] X. Li, W. Cai, J. An, S. Kim, J. Nah, D. Yang, R. Piner, A. Velamakanni, I. Jung, E. Tutuc, Science 324 (2009) 1312.
[25] H. Tamai, T. Kakii, Y. Hirota, T. Kumamoto, H. Yasuda, Chem. Mater. 8 (1996) 454.
[26] T.-Y. Ma, L. Liu, Z.-Y. Yuan, Chem. Soc. Rev. 42 (2013) 3977.
[27] H. Osman, M.H. Zakaria, Polym.-Plast. Technol. Eng. 51 (2012) 243.
[28] S. Yu, D. Liu, S. Zhao, B. Bao, C. Jin, W. Huang, H. Chen, Z. Shen, RSC Adv. 5 (2015) 30943.
[29] J. Tey, M. Careem, M. Yarmo, A. Arof, Ionics (2016) 1.
[30] D. Liu, S. Yu, Y. Shen, H. Chen, Z. Shen, S. Zhao, S. Fu, Y. Yu, B. Bao, Ind. Eng. Chem. 54 (50) (2015) 12570–12579.
[31] X. Wang, G. Sun, P. Routh, D.-H. Kim, W. Huang, P. Chen, Chem. Soc. Rev. 43 (2014) 7067.
[32] N. Mubarak, R. Alicia, E. Abdullah, J. Sahu, A.A. Haslija, J. Tan, J. Environ. Chem. Eng. 1 (2013) 486.
[33] N. Mubarak, R. Thines, N. Sajuni, E. Abdullah, J. Sahu, P. Ganesan, N. Jayakumar, Korean J. Chem. Eng. 31 (2014) 1582.
[34] C.h. Chen, J.C. LaRue, R.D. Nelson, L. Kulinsky, M.J. Madou, J. Appl. Polym. Sci. 125 (2012) 3134.
[35] D.-W. Wang, F. Li, J. Zhao, W. Ren, Z.-G. Chen, J. Tan, Z.-S. Wu, I. Gentle, G.Q. Lu, H.-M. Cheng, ACS Nano 3 (2009) 1745.
[36] T.C. Chandra, M.M. Mirna, J. Sunarso, Y. Sudaryanto, S. Ismadji, J. Taiwan Inst. Chem. Eng. 40 (2009) 457.
[37] D. Mohan, S. Rajput, V.K. Singh, P.H. Steele, C.U. Pittman, J. Hazard. Mater. 188 (2011) 319.
[38] M.A. Ahmad, N. Ahmad, O.S. Bello, Appl. Water Sci. (2014) 1.
[39] X. Diao, P.B. Hazll, D. Resnick, J. Thurlow, The role of agriculture in development; Implications for sub -Saharan Africa, Int. Food Policy Res. Inst. 53 (2007).
[40] N. Cao, H. Darmstadt, F. Soutric, C. Roy, Carbon 40 (2002) 471.
[41] H.M. Santos, C. Lodeiro, J.-L. Capelo-Martínez, Ultrasound in Chemistry, Wiley-VCH Verlag GmbH & Co. KGaA, 2009, pp. p1.
[42] H. Sun, W.C. Hockaday, C.A. Masiello, K. Zygourakis, Ind. Eng. Chem. Res. 51 (2012) 3587.
[43] J. Bréger, M. Jiang, N. Dupré, Y.S. Meng, Y. Shao-Horn, G. Ceder, C.P. Grey, J. Solid State Chem. 178 (2005) 2575.
[44] D. Mohan, A. Sarswat, Y.S. Ok, C.U. Pittman Jr., Bioresour. Technol. 160 (2014) 191.
[45] H.E. Swanson, E. Tatge, R.K. Fuyat, 2, 65, 1953.
[46] B.Y. Yu, S.-Y. Kwak, Mater. Chem. 20 (2010) 8320–8328.
[47] M.A. Abdalla, M.H. Jaafar, Z.A. Al-Othman, S.M. Alfadul, M. Ali Khan, Arab. J. Chem. 4 (2011) 235.
[48] P. Sun, C. Hui, R. Azim Khan, J. Du, Q. Zhang, Y.-H. Zhao, Sci. Rep. 5 (2015) 12638.
[49] S.A. Baig, T. Sheng, C. Sun, X. Xue, L. Tan, X. Xu, PLoS One 9 (2014) e100704.
[50] N. Du, Y. Xu, H. Zhang, C. Zhai, D. Yang, Nanoscale Res. Lett. 5 (2010) 1295.
[51] H. Chaudhari, D. Kelkar, J. Appl. Polym. Sci. 62 (1996) 15.
[52] A. Gök, M. Omastová, J. Prokeš, Eur. Polym. J. 43 (2007) 2471.
[53] J. Zhang, L.-B. Kong, B. Wang, Y.-C. Luo, L. Kang, Synth. Met. 159 (2009) 260.
[54] B. Chen, Z. Chen, S. Lv, Bioresour. Technol. 102 (2011) 716.
[55] K. Kante, E. Deliyanni, T.J. Bandosz, J. Hazard. Mater. 165 (2009) 704.
[56] W. Wang, X. Wang, X. Wang, L. Yang, Z. Wu, S. Xia, J. Zhao, J. Environ. Sci. 25 (2013) 1726.
[57] W.-J. Liu, K. Tian, Y.-R. He, H. Jiang, H.-Q. Yu, Environ. Sci. Technol. 48 (2014) 13951.
[58] N. Leddy, Surface area and porosity, 1-28, 2012.
[59] Z. Zhang, X. Wang, Y. Wang, S. Xia, L. Chen, Y. Zhang, J. Zhao, J. Environ. Sci. 25 (2013) 1044.
[60] Z. Liu, F.-S. Zhang, R. Sasai, Chem. Eng. J. 160 (2010) 57.
[61] J. Sun, X. Sun, H. Zhao, R. Sun, Polym. Degrad. Stab. 84 (2004) 331.
[62] A. Mandal, D. Chakrabarty, Carbohydr. Polym. 86 (2011) 1291.
[63] I. Spiridon, C.A. Teaca, R. Bodîrlău, BioResources 6 (2011) 400.
[64] P. Penjumras, R.B.A. Rahman, R.A. Talib, K. Abdan, Agric. Agric. Sci. Procedia 2 (2014) 237.
[65] C. Rao, R. Venkataraghavan, T. Kasturi, Can. J. Chem. 42 (1964) 36.
[66] S. Ramesh, M. Chai, Mater. Sci. Eng.: B 139 (2007) 240.
[67] W. Liu, J. Kumar, S. Tripathy, K.J. Senecal, L. Samuelson, J. Am. Chem. Soc. 121 (1999) 71.
[68] E.T. Kang, K.G. Neoh, K.L. Tan, Prog. Polym. Sci. 23 (1998) 277.
[69] C. Cui, Y. Du, T. Li, X. Zheng, X. Wang, X. Han, P. Xu, J. Phys. Chem. B 116 (2012) 9523.
[70] C. Yang, J. Du, Q. Peng, R. Qiao, W. Chen, C. Xu, Z. Shuai, M. Gao, J. Phys. Chem. B 113 (2009) 5052.
[71] S. Xuan, Y.-X.J. Wang, J.C. Yu, K.C.-F. Leung, Langmuir 25 (2009) 11835.
[72] J. Deng, C. He, Y. Peng, J. Wang, X. Long, P. Li, A.S. Chan, Synth. Met. 139 (2003) 295.
[73] K. Singh, A. Ohlan, R. Kotnala, A. Bakhshi, S. Dhawan, Mater. Chem. Phys. 112 (2008) 651.
[74] X. Lu, H. Mao, D. Chao, W. Zhang, Y. Wei, J. Solid State Chem. 179 (2006) 2609.
[75] J. Deng, X. Ding, W. Zhang, Y. Peng, J. Wang, X. Long, P. Li, A.S. Chan, Polymer 43 (2002) 2179.
[76] P. Xu, X. Han, C. Wang, B. Zhang, X. Wang, H.L. Wang, Macromol. Rapid Commun. 29 (2008) 1392.
[77] P. Dallas, N. Moutis, E. Devlin, D. Niarchos, D. Petridis, Nanotechnology 17 (2006) 5019.
[78] W. Yan, X. Shuangxi, J. Shengyu, Z. Teili, Z. Chun, e-Polymers 7 (2007) 1187.
[79] L. Kong, X. Lu, W. Zhang, J. Solid State Chem. 181 (2008) 628.
[80] P.M. Grant, I.P. Batra, Solid State Commun. 29 (1979) 225.
[81] J. Fink, H. Fark, N. Nücker, B. Scheerer, G. Leising, R. Weizenhöfer, Synth. Met. 17 (1987) 377.
[82] S. De, A. Dey, S. De, Eur. Phys. J. B—Condens. Matter Complex Syst. 46 (2005) 355.
[83] S.H. Son, H.J. Lee, Y.J. Park, J.H. Kim, Polym. Int. 46 (1998) 308.
[84] B.E. Conway, Electrochemical Supercapacitors: Scientific Fundamentals and Technological Applications, Springer Science & Business Media, 2013.
[85] H. Jin, X. Wang, Y. Shen, Z. Gu, J. Anal. Appl. Pyrolysis 110 (2014) 18.
[86] Z. Lei, X. Sun, H. Wang, Z. Liu, X. Zhao, ACS Appl. Mater. Interfaces 5 (2013) 7501.
[87] Q. Zhang, Y. Li, Y. Feng, W. Feng, Electrochim. Acta 90 (2013) 95.
[88] Q. Hao, X. Xia, W. Lei, W. Wang, J. Qiu, Carbon 81 (2015) 552.
[89] Z. Fan, J. Yan, T. Wei, L. Zhi, G. Ning, T. Li, F. Wei, Adv. Funct. Mater. 21 (2011) 2366.
[90] M. Giovanela, E. Parlanti, E. Soriano-Sierra, M. Soldi, M. Sierra, Geochem. J. 38 (2004) 255.
[91] H. Chen, G. Lin, X. Wang, Y. Chen, Y. Liu, H. Yang, J. Shao, J. Renewable Sustainable Energy 8 (2016) 013112.
[92] R. Krishni, K. Foo, B. Hameed, Desalin. Water Treat. 52 (2014) 6712.
[93] N.M. Mubarak, Y.T. Fo, H.S. Al-Salim, J.N. Sahu, E.C. Abdullah, S. Nizamuddin, N.S. Jayakumar, P. Ganesan, Int. J. Nanosci. 14 (2015) 1550009.
[94] J. Goel, K. Kadirvelu, C. Rajagopal, V.K. Garg, J. Hazard. Mater. 125 (2005) 211.
[95] M. Matias, M. De La Orden, C.G. Sánchez, J.M. Urreaga, J. Appl. Polym. Sci. 75 (2000) 256.
[96] F.B. Reig, J.G. Adelantado, M.M. Moreno, Talanta 58 (2002) 811.
[97] K.R. Prasad, N. Munichandraiah, J. Power Sources 112 (2002) 443.
[98] L. Li, S. Dong, X. Chen, P. Han, H. Xu, J. Yao, C. Shang, Z. Liu, G. Cui, J. Solid State Electrochem. 16 (2012) 877.
[99] X. Xia, Q. Hao, W. Lei, W. Wang, H. Wang, X. Wang, J. Mater. Chem. 22 (2012) 8314.
[100] Z.-A. Hu, Y.-L. Xie, Y.-X. Wang, L.-P. Mo, Y.-Y. Yang, Z.-Y. Zhang, Mater. Chem. Phys. 114 (2009) 990.
[101] J.J. Cai, L.B. Kong, J. Zhang, Y.C. Luo, L. Kang, Chin. Chem. Lett. 21 (2010) 1509.

Please cite this article in press as: K.R. Thines, et al., A new route of magnetic biochar based polyaniline composites for supercapacitor electrode materials, J. Anal. Appl. Pyrol. (2016), http://dx.doi.org/10.1016/j.jaap.2016.08.004